



Contents lists available at ScienceDirect

Journal of Sound and Vibration

journal homepage: www.elsevier.com/locate/jsv



A dual-functional metamaterial for integrated vibration isolation and energy harvesting

Ze-Qi Lu^{*}, Long Zhao, Hu Ding, Li-Qun Chen

Shanghai Institute of Applied Mathematics and Mechanics, Shanghai Key Laboratory of Mechanics in Energy Engineering, School of Mechanics and Engineering Science, Shanghai University, 99 Shangda Road, Shanghai 200444, China



ARTICLE INFO

Keywords:

Nonlinear vibration
Energy harvesting
Vibration isolation
Dual-functional metamaterial

ABSTRACT

Enhancing vibration isolation with locally resonant metamaterials has attracted wide attention due to low-frequency band-gap. Moreover, nonlinear periodic structure could improve the range of targeted energy transfer. In this paper, we propose a dual-functional metamaterial for integrated low-frequency vibration isolation and energy harvesting. A periodic array of nonlinear electrical energy harvesters, realized by implanting a rolling-ball with coils into a spherical magnetic cavity, is explored to isolate mechanical wave and simultaneously harvest electrical energy. The dynamical equation is established for a nonlinear dual-functional metamaterial beam under transverse excitation. The Extended Bloch's theorem is applied to give the dispersion relation. Numerical results obtained by finite element method supported the analytical results. Compared to the narrow band-gaps in metamaterials with spherical magnetic cavity, our numerical analysis demonstrates that a cavity mass arrayed beam with a periodic array of nonlinear energy harvesters has more and wider low-frequency band-gaps. Frequency response functions of output power are derived by using finite element analysis. The harvested power is considerable at the local resonant band-gap. Parameter study demonstrates that increasing the cell size and increasing cavity mass could improve elastic waves isolation performance at low frequencies; Increasing the mass of the rolling-ball in the resonator can significantly decrease the frequency of the local resonance band-gap. The existence of multiple band-gaps could be designed for dual-functional vibration attenuation and energy harvesting. Finally, an experimental rig is designed to validate the theoretical results.

1. Introduction

Metamaterials are man-made heterogeneous materials that exhibit new properties precluded by physical constraints from occurring in the conventional materials. For example, acoustic metamaterials composed of subwavelength structures have band-gaps that can prohibit acoustic or elastic wave propagation [1–10]. Therefore, metamaterial designing is regarded as a promising method for dynamic applications including mechanical wave attenuation, wave guiding, low-frequency vibration isolation, absorption, and energy harvesting [11–16]. As an extension of the aforementioned functions, the dual-functional metamaterials, which can be applied in multi-physics fields, are the focus of this work. Combining energy harvesting and vibration isolation not only enhances vibration isolation but also converts potentially harmful vibration energy into more useful electric energy usable for power devices [17–21].

* Corresponding author.

E-mail address: luzeqi@shu.edu.cn (Z.-Q. Lu).

However, only very few studies on dual-functional metamaterials with integrated vibration isolation and energy harvesting have been reported so far [22–24].

First, we briefly review some previous work using metamaterials with cavity mass for applications of vibration control. Metamaterials behaving like a continuous medium with unusual features were explored by Liu et al. [25]. For example, the positioning dipolar locally resonant metamaterials into a bulk medium emerged a negative effective mass density [26]. Furthermore, embedding monopolar resonators inside a host structure realized a negative stiffness [27]. The studies are further divided into two types: Bragg scattering type and locally resonating type. The former is mainly due to the periodicity of the structure [28–31], while the latter is mainly owing to the resonance characteristics of each unit. The attached local resonance system that could reduce the frequency of the band-gap compared to the Bragg scattering metamaterials without local resonance, has been received wide attention. For example, metamaterials with additional mass-spring-damping resonators [32–35], metamaterials with negative stiffness [36,37], metamaterials with high-static-low-dynamic-stiffness [38–41], metamaterials with attached lateral local resonators [42], metamaterials which has two-dimensional [43], metamaterials which negative mass density. To improve tunable wave manipulation capability, Chen et al. [44] experimentally fabricated an adaptive hybrid acoustic metamaterial which has negative mass density. The results demonstrated that the negative mass could improve tunable energy transfer. In summary, metamaterials with cavity mass has been applied effectively in vibration control.

In the meantime, nonlinear analysis could be a promising method for enhancing properties of an acoustic metamaterial. Gendelman [45] proposed a cubic nonlinear stiffness oscillator (called nonlinear energy sink) coupled to the elastic structure, the transient impact energy in the structure could be localized to the nonlinear additional mass by means of passive energy transmission, thus effectively suppressing the transient vibration of the main structure. Wierschem [46] proposed a large-scale nonlinear energy sink (NES) for explosion shock isolation. Under the impact of such shock waves, the structure can generate high amplitude response and thus cause damage. However, when the NES are coupled in the host structure, the transient energy in the host structure could be rapidly transferred to the NES to rapidly attenuate the vibration of the main structure. Romeo et al. [47] and Manevitch et al. [48] simultaneously proposed the bi-stable NES structure. The steady-state transition of the bistable NES improves the range of targeted energy transfer (TET). The study on the mechanism of NES structure and its TET has laid a theoretical foundation for the design of metamaterial structure with shock-wave regulation characteristics. The metamaterial of spherical particles arranged by squeezing each other is a nonlinear periodic structure that is more thoroughly studied. Donahue [49] designed an underwater acoustic prism for focusing and imaging by using two-dimensional acoustic metamaterial. The nonlinear subwavelength structure based on the NES design is explored to achieve heavy damping and efficient TET effect to control transient stress-wave propagation, thus achieving shock-isolation, which is a disruptive innovation. However, this research has not been carried out effectively.

Multifunctional metamaterial design that not only convert harmful vibration into electric energy to power the wireless sensor, but it also could enhance vibration reduction performance. Therefore, metamaterial designing for the dual functions has been investigated in consideration of the hybrid external conditions. Li et al. [50] designed a dual functional metamaterial for both heat and electric cloak by implanting the non-spherical nano-particles into a cylinder structure. Shen et al. [51] experimentally studied a dual functional metamaterial for both thermal cloak and concentrator by assembling shape-memory-alloy and isotropic-material together. Wiercigroch et al. [52, 53] and Najdecka et al. [54] studied the dynamics of a spherical pendulums system operating in rotational regime with a view of energy harvesting. The thermo-acoustic metamaterial proposed by Maldovan [55] successfully gives Bragg scattering for wave isolation and heat flux. Inspired by the abovementioned studies, it is anticipated that the double functional metamaterial can be designed, which could be employed to control two-physical waves propagation simultaneously [22–24]. Considerable progress has recently been achieved to the investigation of integrated vibration isolation and energy harvesting in metamaterials. However, only linear acoustic metamaterials were studied although nonlinear metamaterials and nonlinear electronic devices offer superior interesting wave propagation phenomena and broadband energy harvesting.

In this manuscript, we arrange a periodic array of electrical energy harvesters, realized by implanting a rolling-ball with coils into a free-moving spherical magnetic cavity on a beam to create band-gaps for wave isolation and produce electrical energy. Compared to conventional periodic attachments, the cavity mass leads to well-separated band-gaps on the host structure due to the array of spherical magnetic cavity. We will show that, through the periodic rolling-balls, both multiple low-frequency isolation band-gaps and energy harvesting can be obtained. The parameters are optimized for improving both vibration isolation and electrical energy

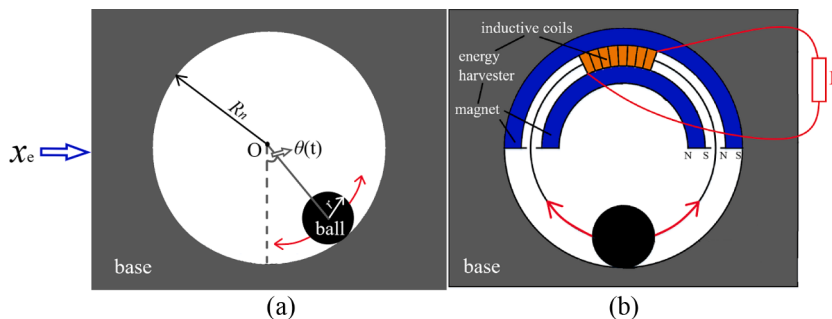


Fig. 1. (a) A nonlinear resonator via a rolling-ball sliding in a spherical cavity; (b) A spherical pendulum energy harvester.

harvesting. Compared to the band-gaps in metamaterials with spherical cavity, a cavity mass arrayed beam with a periodic array of nonlinear energy harvesters has multiple wide band-gaps and low-frequency band-gaps. At the same time, a metamaterial beam experiment was designed to validate the corresponding band-gap characteristics.

2. Description of a dual-functional acoustic metamaterial beam

2.1. A spherical pendulum energy harvester

The mechanical model of a nonlinear spherical pendulum resonator is shown in Fig. 1 which comprises a rolling-ball mass, a base with a spherical cavity, and an energy harvesting device fixed on the base (the coils connected to the rolling-ball can slide). Transverse wave propagation of the acoustic metamaterial can drive the nonlinear spherical pendulum energy harvester. When the spherical cavity has a displacement excitation on the rolling-ball, the rolling-ball slides along the inner surface of the spherical cavity, resulting in inductance coil moving along the magnet trough, which leads to electromagnetic induction of coils generating energy.

When the resonator subject to a horizontal displacement excitation of $x_e = X_e \cos(\omega t)$. The governing equation for a nonlinear spherical pendulum resonator can be achieved via the Lagrange equation

$$\frac{\partial}{\partial t} \left(\frac{\partial L}{\partial \dot{\theta}(t)} \right) - \frac{\partial L}{\partial \theta(t)} = 0 \quad (1)$$

where $L = T - U$, T is the kinetic energy, U is the potential energy. The kinetic energy T of the rolling-ball is

$$T = \frac{1}{2} m_1 \left(R_b^2 \frac{d\theta(t)^2}{dt} + X_e^2 \omega^2 \sin^2 \omega t + 2R_b \frac{d\theta(t)}{dt} X_e \omega \sin \omega t \sin \theta(t) \right) \quad (2)$$

where $m_1 = \frac{4\pi r^3 \rho_1}{3}$ is the mass of the rolling-ball; $\theta(t)$ is the rotation angle of the rolling-ball over time; ρ_1 is the density of the rolling-ball; g is the gravity acceleration; r is the radius of the rolling-ball; R_n is the radius of the curved base; R_b is the distance between the centre of the rolling-ball and the centre of the curved base ($R_b = R_n - r$).

The horizontal plane where the centroid O of spherical cavity is in Fig. 1(b) is the zero potential energy surface, the potential energy U of the rolling-ball is

$$U = -m_1 g R_b \cos \theta(t) \quad (3)$$

L can be written as

$$L = T - U = \frac{1}{2} m_1 \left(R_b^2 \frac{d\theta(t)^2}{dt} + X_e^2 \omega^2 \sin^2 \omega t + 2R_b \frac{d\theta(t)}{dt} X_e \omega \sin \omega t \sin \theta(t) \right) + m_1 g R_b \cos \theta(t) \quad (4)$$

Substituting Eq. (4) into Lagrange equation Eq. (1). The dynamic equation of the rolling-ball is given by

$$\frac{d^2 \theta(t)}{dt^2} + \left(\frac{X_e \omega^2}{R_b} \cos \omega t + \frac{g}{R_b} \right) \sin \theta(t) = 0 \quad (5)$$

The energy harvesting device is added to the resonator cavity. According to Kirchhoff's law, the dynamic equation of the resonator with the energy harvesting can be given by

$$\begin{cases} \frac{d^2 \theta(t)}{dt^2} + \left(\frac{X_e \omega^2}{R_b} \cos \omega t + \frac{g}{R_b} \right) \sin \theta(t) - \frac{BL_{\text{coil}}}{m_1} i(t) = 0 \\ \frac{di(t)}{dt} + \frac{R}{L_{\text{ind}}} i(t) + \frac{BL_{\text{coil}} R_b}{L_{\text{ind}}} \frac{d\theta(t)}{dt} = 0 \end{cases} \quad (6)$$

where B is magnetic induction intensity; $i(t)$ is the current generated in the induction coil; R is the resistance in the energy harvesting circuit; L_{ind} is the inductance strength; L_{coil} is the coil length.

Taylor expansion of $\sin \theta(t)$ in Eq. (6), the equation of the motion can be given by

$$\begin{cases} \frac{d^2 \theta}{dt^2} + \left(\frac{X_e \omega^2}{R_b} \cos \omega t - \frac{g}{R_b} \right) \left(\theta(t) + \frac{\theta^3(t)}{6} \right) - \frac{BL_{\text{coil}}}{m_1} i(t) = 0 \\ \frac{di(t)}{dt} + \frac{R}{L_{\text{ind}}} i(t) + \frac{BL_{\text{coil}} R_b}{L_{\text{ind}}} \frac{d\theta(t)}{dt} = 0 \end{cases} \quad (7)$$

After obtaining the Eq. (7), the amplitude-frequency response of the resonance system is analyzed by using the generalized harmonic balance method in this paper. The generalized displacement of the ball and the harvested current term are expanded into Fourier series respectively:

$$\theta_n(t) = a_{1,0} \sum_{i=1}^n [a_{1,i} \cos(i\omega t) + b_{1,i} \sin(i\omega t)] \quad (8a)$$

$$i_n(t) = a_{2,0} + \sum_{i=1}^n [a_{2,i}\cos(i\omega t) + b_{2,i}\sin(i\omega t)] \quad (8b)$$

where n is the harmonic order, the quantities $a_{1,0}, a_{1,i}, b_{1,i}$ and $a_{2,0}, a_{2,i}, b_{2,i}$ are the coefficients to be determined for the corresponding harmonic terms.

Substituting Eq. (8) into Eq. (7) and balancing the coefficients of harmonic terms $\theta_n(t)$ and $i_n(t)$, a series of algebraic equations of the coefficients of harmonic terms can be obtained, and the amplitude-frequency response curve of the nonlinear resonator can be obtained by arc-length continuation method.

To obtain the amplitude-frequency response curves using the harmonic balance method, convergence analysis of the analytical solutions are conducted in this paper. Fig. 2 shows comparison of the amplitude-frequency response curves between the nonlinear resonator with 3rd order and 5th-order truncations. It can be observed, that for the parameters chosen, there is good agreement between the 3rd-order and 5th-order harmonic truncation results. Therefore the 3rd-order harmonics truncation can be used for further investigation of the dynamic behavior.

Fig. 3 shows the amplitude-frequency response curves under the parameters of amplitude of the excitation X_e and the amplitude-excitation amplitude response curves under different frequency of the excitation ω . It is found that the response curve of the nonlinear spherical pendulum resonator bends to the left in the frequency interval near the resonance frequency, when the system presents a softening nonlinearity. As the amplitude of excitation X_e increases, the response amplitude of the nonlinear spherical pendulum resonator near the resonance frequency increases. In particular, within the excitation amplitude of 0.01–0.018m, the response amplitude appears a multi-value state, which reflects the nonlinear system of the resonator.

In short, this section mainly introduces the nonlinear dynamics characteristic of the spherical pendulum resonator, which provides a theoretical basis for introducing the nonlinear resonator into the acoustic metamaterial creates a local resonance band-gap to enhance the propagation suppression of elastic waves and energy harvesting.

2.2. Modelling of a dual-functional acoustic metamaterial beam

This section models and analyzes the dual-functional metamaterial beams using the theory of multi-physics to explore the construction of a new dual-functional acoustic metamaterial by integrating the cavity mass metamaterial with the local nonlinear energy harvester for both low-frequency vibration isolation and energy harvesting. The schematic of the dual-functional acoustic metamaterial beam is shown in Fig. 4.

As shown in Fig. 4, periodically arrayed energy harvesters are positioned to the acoustic metamaterial beam with periodically arrayed spherical cavity. When the wave propagated through the dual-functional metamaterials, local resonances are generated, thus preventing the propagation of low frequency elastic wave and realizing the passive control of vibration. When displacement excitation x_e occurs, the rolling-ball sliding back and forth on the inner surface of the spherical cavity, and simultaneously drives the coils to cutting the magnetic field, resulting in energy harvest. This paper covers the energy generated by vibration of the dual-functional acoustic metamaterial beam, and compares the low-frequency vibration isolation of the dual-functional acoustic metamaterial beam with or without energy harvesting device.

This section presents the derivation of the dynamic equations for a dual-functional acoustic metamaterial beam. The dual-functional acoustic metamaterial beam proposed in this paper is shown in Fig. 4 (c). Based on periodically arrayed cavity masses, energy harvesting resonators are positioned to realize the dual-function of low-frequency vibration isolation and energy harvesting.

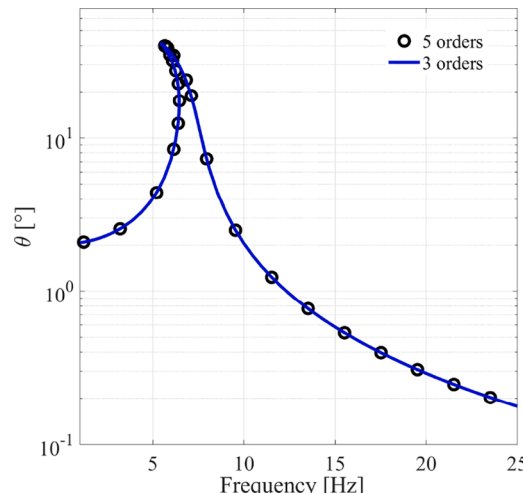


Fig. 2. Amplitude-frequency response curves under different harmonic order truncations.

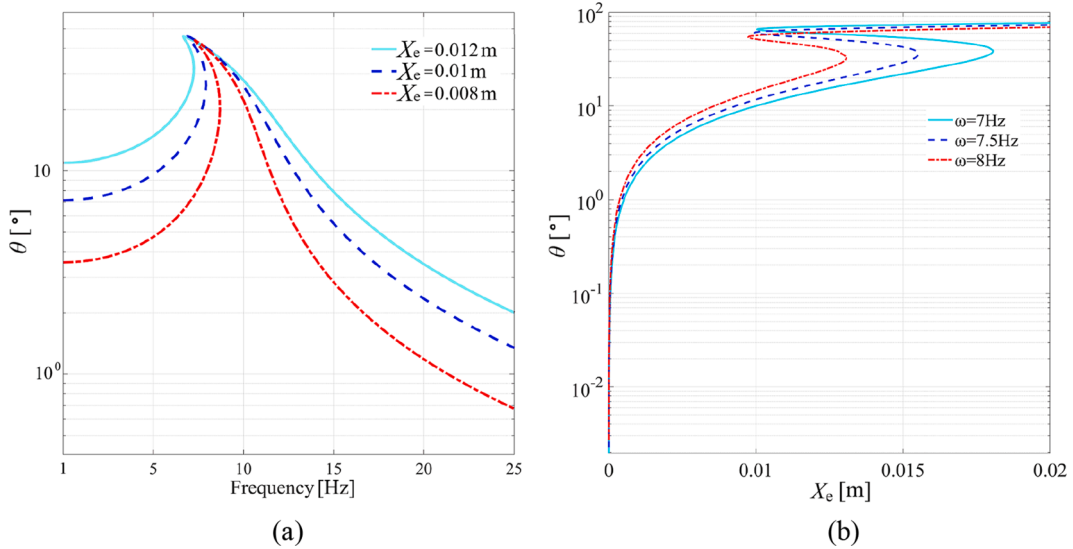


Fig. 3. (a) Amplitude-frequency response curves of the nonlinear spherical pendulum resonator under different displacement excitation X_e ; (b) Amplitude-excitation amplitude response curves of the nonlinear spherical pendulum resonator at different frequencies ω . The parameters are: $R_b = 0.015\text{ m}$, $R = 1\Omega$, $L_{\text{ind}} = 0.5\text{ H}$, $L_{\text{coil}} = 0.1\text{ m}$, $\rho_1 = 7780\text{ kg/m}^3$, $r = 0.01\text{ m}$ and $B = 0.5\text{ B}$.

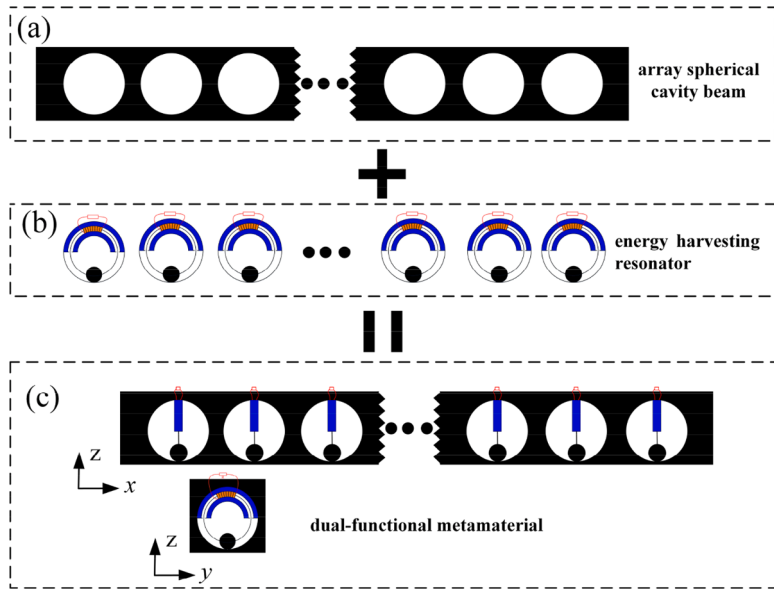


Fig. 4. (a) View of the structure of the array spherical cavity beam; (b) View of the structure of the local nonlinear energy harvesting resonator; (c) View of the structure of the dual-functional metamaterial beam.

The main component of the acoustic metamaterial studied in this paper is an infinite-long beam.

When a beam with a height to length ratio less than 1:5 is excited transversely, the effect of moment of inertia around the neutral axis of the cross section need to be considered. Therefore, the typical crystal cell of this metamaterial beam is equivalent to a Timoshenko beam in this study.

For the metamaterial beam with equivalent Timoshenko beam, l is the unit cell length; A is the cross-sectional area; I is the moment of inertia of the section; ρ is the density of the material; E is tensile elastic modulus; G is the modulus of shear elasticity. As shown in the Fig. 5, the transverse displacement of the neutral axis of the cross section with time change t is denoted as $w(x, t)$; The shear angle of the beam section changing with time t is denoted as $\gamma(x, t)$; The total bending deformation angle of metamaterial beam is denoted as $\theta_f(x, t)$.

$$\theta_f(x, t) = \frac{\partial w(x, t)}{\partial x} + \gamma(x, t) \quad (9a)$$

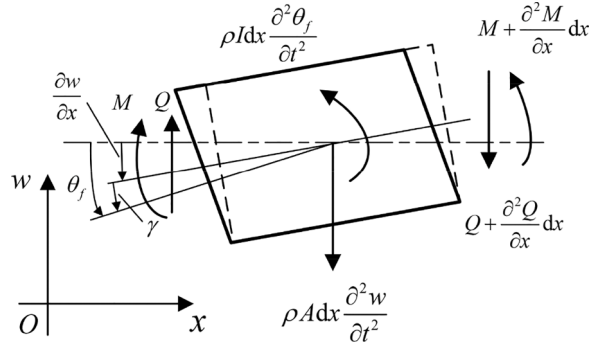


Fig. 5. The infinitesimal analysis of Timoshenko beams.

$$M(x, t) = EI \frac{\partial^2 w(x, t)}{\partial x^2} \quad (9b)$$

$$Q(x, t) = \beta GA \gamma(x, t) \quad (9c)$$

where, $M(x, t)$ is the bending moment acting on the beam section; $Q(x, t)$ is the shear stress acting on the beam section. Eq. (9a) and Eq. (9b) give the relationship between the shear stress $Q(x, t)$ and the shear angle of the beam section $\theta_f(x, t)$.

$$Q(x, t) = \beta GA \left[\theta_f(x, t) - \frac{\partial w(x, t)}{\partial x} \right] \quad (10)$$

Based on the theorem of centroid motion and the theorem of moment of momentum, the dynamic equation of Timoshenko beam could be obtained.

$$\begin{cases} \rho A \frac{\partial^2 w(x, t)}{\partial t^2} + \beta GA \left[\frac{\partial \theta(x, t)}{\partial x} - \frac{\partial^2 w(x, t)}{\partial x^2} \right] = 0 \\ \rho I \frac{\partial^2 \theta(x, t)}{\partial t^2} - EI \frac{\partial^2 \theta(x, t)}{\partial x^2} + \beta GA \left[\theta_f(x, t) - \frac{\partial w(x, t)}{\partial x} \right] = 0 \end{cases} \quad (11)$$

The dynamic equation is a set of second-order partial differential equations for the transverse displacement $w(x, t)$ and rotation angle $\theta_f(x, t)$ of the metamaterial beam. The fourth-order partial differential equation containing only the transverse displacement $w(x, t)$ of the metamaterial beam can be obtained through differential variation.

$$\rho A \frac{\partial^2 w(x, t)}{\partial t^2} + EI \frac{\partial^4 w(x, t)}{\partial x^4} - \rho I \frac{\partial^4 w(x, t)}{\partial x^2 \partial t^2} - \frac{\rho IE}{\beta G} \frac{\partial^4 w(x, t)}{\partial x^2 \partial t^2} + \frac{\rho^2 I}{\beta G} \frac{\partial^4 w(x, t)}{\partial t^4} = 0 \quad (12)$$

where β is the shear stress coefficient related to the cross-section, the cross-section of the metamaterial beam is a rectangle.

Based on Newton's second law, for the metamaterial beam with resonator attached in the cavity of periodic array, when it is transverse excitation, the governing equation of bending wave propagation in the main beam can be given by

$$\rho A \frac{\partial^2 w(x, t)}{\partial t^2} + EI \frac{\partial^4 w(x, t)}{\partial x^4} - \rho I \frac{\partial^4 w(x, t)}{\partial x^2 \partial t^2} - \frac{\rho IE}{\beta G} \frac{\partial^4 w(x, t)}{\partial x^2 \partial t^2} + \frac{\rho^2 I}{\beta G} \frac{\partial^4 w(x, t)}{\partial t^4} = [R_1(t) + R_2(t)] \delta(x - l) \quad (13)$$

where $R_1(t) + R_2(t)$ is the interaction force between the periodic structure and the main body of the metamaterial beam ($R_1(t)$ is the interaction force between the cavity mass of the metamaterial beam and the main body of the beam; $R_2(t)$ is the interaction between the resonator and the main body of the beam); $\delta(x - l)$ is the Dirichlet function; The interaction forces are $R_1(t), R_2(t)$

$$\begin{cases} R_1(t) = \frac{m_1 g}{R_b} \sin \theta_i(t) \\ R_2(t) = -\frac{4\pi R_n^3 \rho}{3} \frac{\partial^2 w(x, t)}{\partial t^2} \Big|_{x=l} \end{cases} \quad (14)$$

where θ_i is the angle between the spherical pendulum and the equilibrium position in the typical cell when the metamaterial beam receives transverse excitation.

The governing equation of typical unit cell of metamaterial beam can be obtained from the dynamic equation of simultaneous nonlinear resonators

$$\left\{ \begin{array}{l} \rho A \frac{\partial^2 w(x, t)}{\partial t^2} + EI \frac{\partial^4 w(x, t)}{\partial x^4} - \rho I \frac{\partial^4 w(x, t)}{\partial x^2 \partial t^2} - \frac{\rho IE}{\beta G} \frac{\partial^4 w(x, t)}{\partial x^2 \partial t^2} + \frac{\rho^2 I}{\beta G} \frac{\partial^4 w(x, t)}{\partial t^4} \\ \quad - \left[\frac{m_1 g}{R_b} \sin \theta_i(t) - \frac{4\pi R_n^3 \rho}{3} \frac{\partial^2 w(x, t)}{\partial t^2} \right] \delta \left(\frac{l}{2} \right) = 0 \\ \frac{d^2 \theta_i(t)}{dt^2} + \frac{g}{R_b} \sin \theta_i(t) = 0 \end{array} \right. \quad (15)$$

Based on Kirchhoff's law, the dynamic equation of the dual-functional metamaterial beam with the energy harvesting can be given by

$$\left\{ \begin{array}{l} \rho A \frac{\partial^2 w(x, t)}{\partial t^2} + EI \frac{\partial^4 w(x, t)}{\partial x^4} - \rho I \frac{\partial^4 w(x, t)}{\partial x^2 \partial t^2} - \frac{\rho IE}{\beta G} \frac{\partial^4 w(x, t)}{\partial x^2 \partial t^2} + \frac{\rho^2 I}{\beta G} \frac{\partial^4 w(x, t)}{\partial t^4} \\ \quad - \left[\frac{m_1 g}{R_b} \sin \theta_i(t) - \frac{4\pi R_n^3 \rho}{3} \frac{\partial^2 w(x, t)}{\partial t^2} \right] \delta \left(\frac{l}{2} \right) = 0 \\ \frac{d^2 \theta_i(t)}{dt^2} + \frac{g}{R_b} \sin \theta_i(t) - \frac{BL_{\text{coil}}}{m_1} i(t) = 0 \\ \frac{di(t)}{dt} + \frac{R}{L_{\text{ind}}} i(t) + \frac{BL_{\text{coil}} R_b}{L_{\text{ind}}} \frac{d\theta_i(t)}{dt} = 0 \end{array} \right. \quad (16)$$

Fourier expansion of the unknown quantity is carried out and the solution can be given via Bloch's theorem

$$w(x, t) = W_0 e^{i(\omega t - qx)} \quad (17a)$$

$$w(t) = W_0 e^{i\omega t} \quad (17b)$$

$$\theta_i(t) = \Theta_{i0} e^{i\omega t} \quad (17c)$$

$$i(t) = I_0 e^{i\omega t} \quad (17d)$$

where ω is the vibration frequency, q is the wave vector in the x direction. We write the one-dimension vectors q as scalar forms in this paper.

The above governing equation can be applied to the unit cell through which the harmonic bending elastic wave passes

$$\left\{ \begin{array}{l} \int_{-\frac{l}{2}}^{\frac{l}{2}} \left(\rho A \frac{\partial^2 (W_0 e^{i(\omega t - qx)})}{\partial t^2} + \frac{\rho^2 I}{\beta G} \frac{\partial^4 (W_0 e^{i(\omega t - qx)})}{\partial t^4} + \frac{4\pi R_n^3 \rho}{3} \frac{\partial^2 (W_0 e^{i(\omega t - qx)})}{\partial t^2} \right) dx \\ \quad + \int_{-\frac{l}{2}}^{\frac{l}{2}} \left(EI \frac{\partial^4 (W_0 e^{i(\omega t - qx)})}{\partial x^4} - \rho I \frac{\partial^4 (W_0 e^{i(\omega t - qx)})}{\partial x^2 \partial t^2} \right) dx \\ \quad - \int_{-\frac{l}{2}}^{\frac{l}{2}} \left(\frac{\rho IE}{\beta G} \frac{\partial^4 (W_0 e^{i(\omega t - qx)})}{\partial x^2 \partial t^2} \right) dx - \frac{m_1 g}{R_b} \Theta_{i0} e^{i\omega t} = 0 \\ \frac{d^2 \Theta_{i0} e^{i\omega t}}{dt^2} + \frac{g}{R_b} \Theta_{i0} e^{i\omega t} - \frac{BL_{\text{coil}}}{m_1} I_0 e^{i\omega t} = 0 \\ \frac{dI_0 e^{i\omega t}}{dt} + \frac{R}{L_{\text{ind}}} I_0 e^{i\omega t} + \frac{BL_{\text{coil}} R_b}{L_{\text{ind}}} \frac{d\Theta_{i0} e^{i\omega t}}{dt} = 0 \end{array} \right. \quad (18)$$

After integrating Eq. (18), Eq. (18) can be solved by using Euler's formula

$$\left\{ \begin{array}{l} \frac{\rho A W_0 \omega^2}{q} k_T + \frac{2I\rho^2 W_0 \omega^4}{q\beta G} k_T + \frac{8\pi R_n^3 \rho W_0 \omega^2}{3q} k_T + 2EI W_0 q^3 k_T - 2\rho I W_0 \omega^2 q k_T \\ \quad - \frac{2EI\rho W_0 \omega^2 q}{\beta G} k_T - \frac{m_1 g}{R_b} \Theta_{i0} = 0 \\ \Theta_{i0} \omega^2 + \frac{g}{R_b} \Theta_{i0} - \frac{BL_{\text{coil}}}{m_1} I_0 = 0 \\ I_0 \omega + \frac{R}{L_{\text{ind}}} I_0 + \Theta_{i0} \omega \frac{BL_{\text{coil}} R_b}{L_{\text{ind}}} = 0 \end{array} \right. \quad (19)$$

where $k_T = \sin \left(\frac{ql}{2} \right)$. The coefficient matrix can be written as

$$\begin{bmatrix} \Re k_T & -\frac{m_1 g}{R_b} & 0 \\ 0 & \omega^2 + \frac{g}{R_b} & -\frac{BL_{\text{coil}}}{m_1} \\ 0 & \frac{BL_{\text{coil}} R_b \omega}{L_{\text{ind}}} & \frac{R}{L_{\text{ind}}} \end{bmatrix} \times \begin{bmatrix} W_0 \\ \Theta_{i0} \\ I_0 \end{bmatrix} = 0 \quad (20)$$

where $\Re = \frac{\rho A \omega^2}{q} + \frac{2I_p^2 \omega^4}{q \rho G} + \frac{8\pi R_b^3 \rho \omega^2}{3q} + 2EIq^3 - 2\rho I \omega^2 q - \frac{2EI \rho \omega^2 q}{\rho G}$.

By solving the coefficient term of Eq. (20) and making the determinant of the coefficient zero, the relationship between frequency ω and wave vector q can be obtained, which is the energy structure relationship of the metamaterial beam studied in this paper.

2.3. Finite element analysis

The method of finite element is applied to analysis the dynamic equation of the dual-functional metamaterial beam with the additional nonlinear local resonator. Amplitude-frequency response of the dual-functional metamaterial beam composed of 10 cells of the nonlinear local resonator is calculated. A displacement excitation is applied at the one end of the dual-functional metamaterial beam, and the amplitude-frequency response is received through the dual-functional metamaterial beam at the other one end of the beam. Furthermore, the band-gaps of the dual-functional metamaterial beam with the same parameter is calculated and discussed together with the amplitude-frequency response. The unit cell parameters of the dual-functional metamaterial beam are shown in Table 1.

Therefore, the band-gap structure curves of the metamaterial with the additional nonlinear resonator are solved by analytical method and finite element method respectively to examine the relationship between wave vector and frequency. In this work, the element of electromagnetic induction is used for energy harvesting, and the permanent magnets are added to both sides of the unit cell as shown in Fig. 6.

Fig. 6 (a) shows the unit cell plotted in COMSOL according to the size in Table 1. Fig. 6(b) shows the metamaterial unit cell which could realize the function of vibratory energy harvesting. The direction of red arrow in the figure is the direction of magnetic induction line in coupling field. It can be seen that the vibration of the sliding ball in the resonator can move through the cutting magnetic induction line. The implementing could harvest the energy when the sliding ball vibrates.

The Frequency response function matrix can be given by

$$\mathbf{M}[\ddot{p}] + \mathbf{C}(p, \dot{p})[\dot{p}] + \mathbf{K}(p)[p] = \{F\} \quad (21)$$

$$\{F\} = \{il\rho A \omega^2 X_e \cos \omega t, 0, 0, il\rho A \omega^2 X_e \cos \omega t, 0, 0, \dots\}^T \quad (22)$$

$$\{p\} = [-\omega^2 \mathbf{M} + j\omega \mathbf{C} + \mathbf{K}]^{-1} \{F\} \quad (23)$$

where \mathbf{M} , \mathbf{C} , \mathbf{K} represent the mass matrix, damping matrix and stiffness matrix of the discrete finite dual-functional metamaterial beam. i is the number of cells in the infinite period metamaterial beam. $[p]$ and $\{F\}$ represent displacement vector and force vector. The finite element analysis is applied to solve the finite element model, and the amplitude-frequency responses of the dual-functional metamaterial beam are achieved by extracting the dynamic response data at the other end. In this section, the finite element simulation of elastic wave propagation in metamaterial structure is carried out, and the simulation results under different conditions are obtained.

Table 1
Parameters of a dual-functional metamaterial.

Unit cell parameters		Nonlinear resonator parameters			
Item	Notation	Value	Item	Notation	
length	l [m]	0.1	rolling-ball radius	r [m]	0.005
cross-sectional area	A [m^2]	0.0036	density of material	ρ_1 [kg/m^3]	7780
density of material	ρ [kg/m^3]	1800	coil length	L_{coil} [m]	0.1
Young's modulus	E [Pa]	7.6×10^5	resistance	R [Ω]	1
spherical cavity radius	R_n [m]	0.02	magnetic flux	B [T]	0.5
inertia moment	I [m^4]	8.33×10^{-6}	inductance	L_{ind} [H]	0.5
excitation amplitude	X_e [m]	0.01			
shear modulus	G [Pa]	1×10^6			
shear stress coefficient	β	5/6			
Poisson's ratio	ν	0.47			

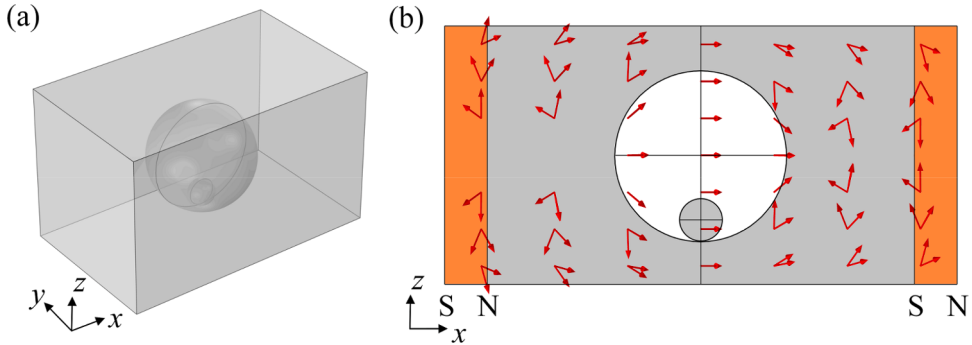


Fig. 6. Finite element model of metamaterial beam with energy harvesting.

3. Results and discussion

This section studies band-gaps of the dual-functional metamaterial. The energy band structures for different conditions are achieved via finite element method. The wave vector q swept from $-\pi/l$ to π/l based on the first Brillouin zone theory.

In Fig. 7, the analytical band-gap structures of typical unit cell obtained by solving Eq. (20) were compared with those obtained by finite element method under COMSOL. By comparing the two calculation results, it is found that the wave vectors q of the two methods are agreement in the primary Brillouin zone. However, it is more convenient to use finite element simulation to calculate the band-gap structure of metamaterial beams in different states. The finite element method is most frequently used method to study metamaterial beams.

3.1. Comparison of band-gaps between with/without nonlinear local resonator

To explore whether the addition of nonlinear local resonator in the metamaterial beams could affect the band-gap and vibration response of the structure, the band-gaps curves and amplitude-frequency response curves of dual-functional metamaterial without nonlinear local resonator (shown in Fig. 8(a) and (b)) and with nonlinear local resonator (shown in Fig. 8(c) and (d)) are compared. The band-gaps of the finite periodic structure are similar to those of the infinite periodic structure. When the period number is very large, the starting and ending frequency of the band-gap tends to the theoretical value of the band-gap, which provides a basis for replacing infinite periodic metamaterial with the finite periodic metamaterial. In theory, vibration could be completely isolated at the frequency range of the forbidden band. However, the results for amplitude-frequency response show that the vibration is still transmitted. The reason for this is that the periodic structure of acoustic metamaterial is infinite in theory, and here the frequency response is obtained by simulation through 10 units. Actually, vibration transmission could be significantly reduced, but not to zero.

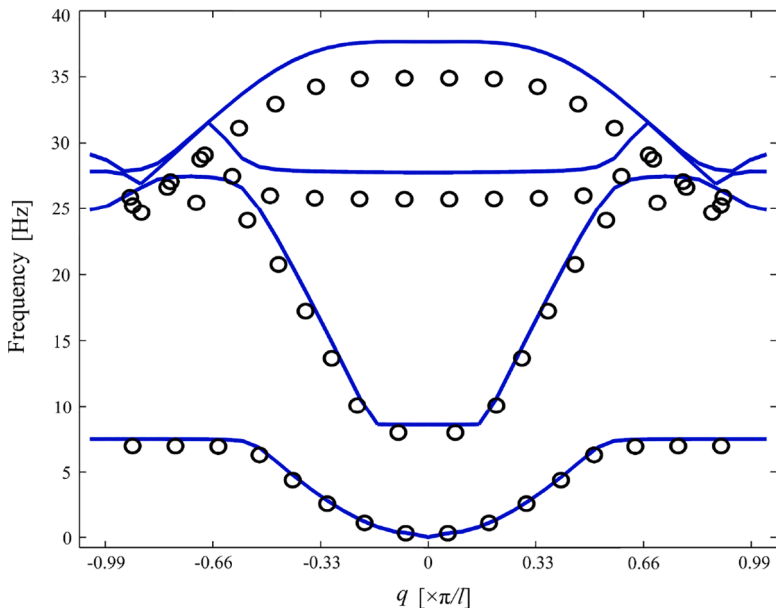


Fig. 7. Analytical solution (black 'o') and finite element solutions (blue line).

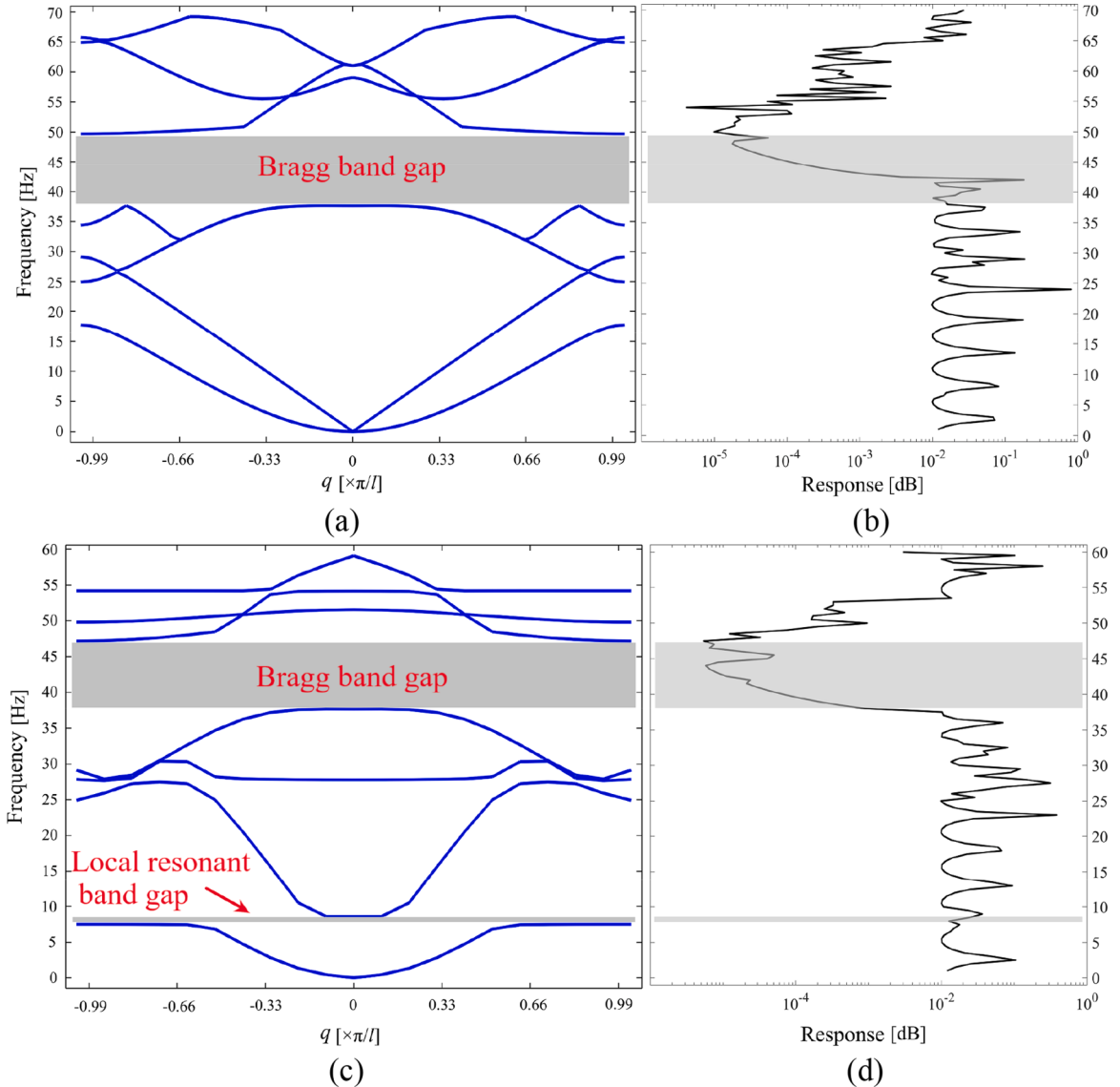


Fig. 8. Band-gaps and amplitude-frequency response of metamaterial. (a) and (b): without nonlinear local resonator; (c) and (d): with nonlinear local resonator. Band-gaps: (a) and (c); amplitude-frequency response: (b) and (d).

Under the same size $0.1m \times 0.06m \times 0.06m$, the band-gap and amplitude-frequency response of the metamaterials with periodic structure only caused by spherical cavity are shown in Fig. 8(a) and (b). It is clearly observed that Bragg band-gap (38Hz-49Hz) exist within the range of (0-60Hz), and the response corresponding to these band-gap frequency range is suppressed. The corresponding response in the band-gap frequency range has a significant decreasing trend compared with the response outside the range. Therefore, the metamaterial is also able to suppress vibration with only spherical cavity arrayed.

Fig. 8(c) and (d) show the band-gaps and amplitude-frequency responses of the metamaterial with both the periodic arrangement of the spherical cavity and the local nonlinear resonator. Within the range of (0-60Hz), there are two band-gaps: the Bragg band-gap (7HZ-8Hz) and the local resonance band-gap (37.5HZ-47Hz) due to the nonlinear resonator. In the plot of amplitude-frequency response, responses of such corresponding frequency ranges are suppressed. As indicated in Fig. 8, the corresponding response in the two band-gap frequency ranges also showed a significant trend of decrease compared with the response outside the range. Therefore, additional nonlinear resonators can improve the vibration isolation performance of metamaterials at low-frequencies.

Compared with the band-gap diagram and the amplitude frequency response diagram in Fig. 8, it can be observed that the frequency range of large vibration attenuation in finite structure is basically consistent with that in infinite structure, which indicates that vibration attenuation is caused by band-gap behavior. Generally, the addition of nonlinear local resonator in metamaterials can significantly reduce the wave propagation range, and the frequencies of the band-gap decreases from (38-49Hz) to (36-46Hz), also a local resonance band-gap (7HZ-8Hz) due to resonator resonance generates in the low-frequency range. In conclusion, nonlinear local

resonator could increase the frequency range of band-gaps, generate a local resonance band-gap to suppress the vibration in the lower frequency range. At the same time, the size of the response is also significantly reduced compared with that without the resonator. Comparison of the band-gaps and the frequency response between with and without local resonator demonstrates that the addition of nonlinear local resonator creates a local resonance band-gap in the low-frequency range and improves the performance of vibration isolation.

Recently, many studies have been carried out to achieve local resonance band-gap and Bragg band-gap via attaching different types of resonators to the beams. Compared with previous studies, this dual-functional metamaterial beam with additional energy harvesting functional resonator has lower frequency local resonance band-gap to isolate vibration at lower frequencies. For example, the central frequency of the local resonance band-gap of metamaterials in reference [42] is 499Hz, and that in this paper is 8Hz.

3.2. Band-gaps of a dual-functional metamaterial beam for different sizes

To examine the effects of the unit cell size, the band-gaps of the dual-functional metamaterial between $0.05m \times 0.03m \times 0.03m$ and $0.1m \times 0.06m \times 0.06m$ are compared with the same material, (The resonator is still in the centroid of the cell) shown in Fig. 9. When the scanning range of wave vector is the same as the first Brillouin zone, the former one has two band-gaps at the frequency range (0-67Hz), the latter one has two band-gaps at the frequency range (0-60Hz). The frequency widths of the Bragg band-gap could increase with the increase of the unit cell size, which also reflects the regulation mechanism of Bragg band-gap from the side. In brief, the band-gaps of the $0.05m \times 0.03m \times 0.03m$ are narrower than that of the $0.1m \times 0.06m \times 0.06m$. By increasing the cell size, the band-gap frequency range can be expanded.

3.3. Band-gaps of a dual-functional metamaterial beam for different materials

To investigate the vibration isolation efficiency of the dual-functional metamaterial with different materials of the bulk, band-gaps of the dual-functional metamaterial structure between Acrylonitrile-Butadiene-Styrene plastic (ABS) and rubber material of the bulk are compared under a cell size of $0.1m \times 0.06m \times 0.06m$. The band-gaps of such two dual-functional metamaterial with different materials of bulk are achieved by finite element method, as shown in Fig. 10. For ABS material, one band-gap (2180Hz-2415Hz) exist at the frequency range (0-3500Hz), when the nonlinear resonator resonates in this frequency range, it could not suppress the elastic wave. Comparison of band-gaps between ABS and rubber material demonstrates that rubber material has lower frequency of the band-gap, and the vibration isolation efficiency of rubber material is significantly better than that of ABS material in the low-frequency range.

3.4. Energy harvesting from a dual-functional metamaterial beam

This section discusses energy harvesting of a dual-functional metamaterial with nonlinear local resonator. The displacement of the rolling-ball in three resonators is obtained via finite element simulation. According to the law of electromagnetic induction, the electromotive force generated in the i -th resonator can be given by

$$E_i(t) = BL_{\text{coil}}\dot{x}_i(t) \quad (24)$$

where \dot{x}_i is the velocity of excitation; $E_i(t)$ is the electromotance generated by the coil cutting magnetic induction line. The power generated by the resonator with the energy harvesting device can be given by

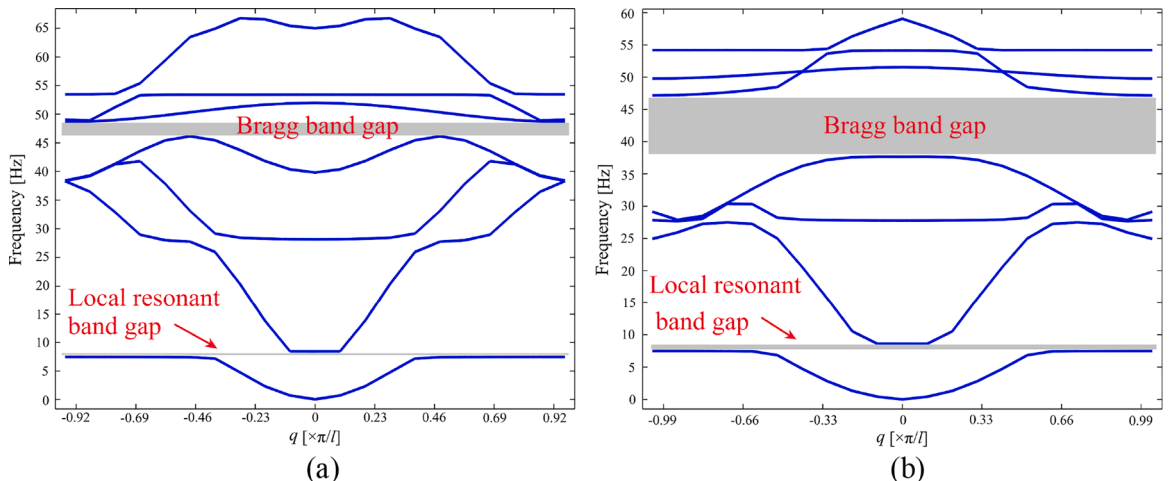


Fig. 9. Band-gaps of the dual-functional metamaterial with different cell size. (a) $0.05m \times 0.03m \times 0.03m$ (b) $0.1m \times 0.06m \times 0.06m$.

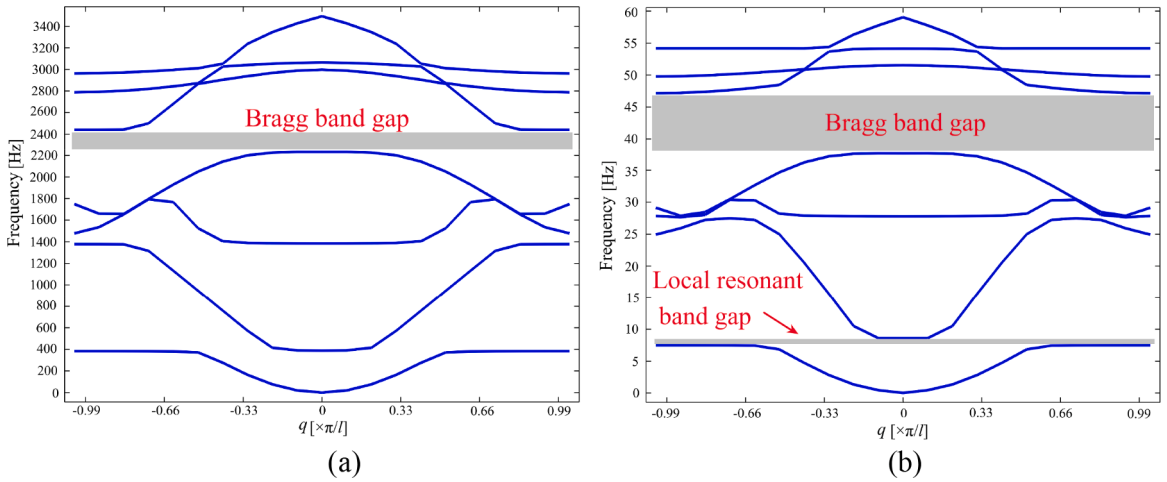


Fig. 10. Band-gaps of the dual-functional metamaterial with different materials of the bulk. (a) ABS material, (b) rubber materials.

$$P_i = \frac{\text{MS}(E_i(t))}{R} \quad (25)$$

where MS is mean-square.

Substituting the displacement of the coils that fixed to the rolling-ball into Eq. (24) and Eq. (25), gives the output power as shown in Fig. 11 by using finite element analysis. The No.1, No.2, and No.3 response curves are the energy of the rolling-ball vibrating in the resonator of the metamaterial beam near the vibration point, the intermediate position resonator, and the resonator on the other side of the metamaterial beam. From the rolling-ball power response curve in the resonator, it can be concluded that the power response curve produces peaks near the frequency of 7Hz-8Hz, which is close to the frequency range of the resonance frequency of the rolling-ball pendulum in a unit resonator previously studied. It can be concluded that the metamaterial beam attached with a nonlinear resonator produces a local resonant band-gap due to resonator resonance. In the frequency range of the local resonance band-gap, the kinetic energy of the metamaterial beam sinks to the resonator via the rolling-ball vibrating in the resonator, then converted the mechanical energy into the electrical energy by the harvester device. Therefore, the vibration of the metamaterial beam attenuates and plays a role of vibration reduction. In Fig. 11, the local resonance frequency band of the band-gap can produce power which even reaches to the peak (4.7 W). The caused by the periodic arrangement of spherical cavity, rolling-ball is in a state of vibration suppression (5.5×10^{-5} W).

4. Analysis of the different parameters

The spherical cavity mass metamaterial beam with an additional nonlinear resonator with energy harvesting device can achieve

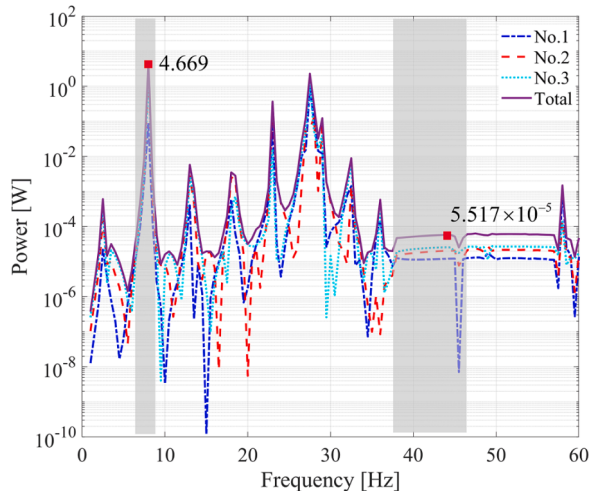


Fig. 11. Frequency response of output power for the dual-functional metamaterial beam.

dual functions of suppressing wave propagation and vibration energy harvesting. This section analyzes the band-gap characteristics of the metamaterial beam structure under different geometrical and physical parameters, including the unit cell size, rolling-ball mass of the resonator and cavity mass.

4.1. Effects of unit cell size

Fig. 12 shows the effect on transverse wave propagation when unit cell size of the metamaterial beam is changed, the nonlinear resonator is at the centroid of the element. It is found that increasing cell size has minimal effects on the range of the low-frequency local resonance band-gap, but reduces the frequency of Bragg band-gap and increase the bandwidth. In particular, the center frequency of the Bragg band-gap decreases from 47Hz to 24.5Hz, and the Bragg bandwidth increases from 2.5Hz to 9Hz, which greatly improves the vibration isolation performance of metamaterials. In conclusion, under certain conditions, the frequency range of the Bragg band-gap can be reduced by increasing the size of unit cell, thereby controlling the elastic wave propagation.

4.2. Effects of rolling-ball mass in each nonlinear resonator

The mass of the rolling-ball in each nonlinear resonator also has a great influence on the band-gap. **Fig. 13** shows the effect on the band-gap generated by the wave propagation in the metamaterial beam when the mass of the rolling-ball in the nonlinear resonator is changed. The unit cell size is fixed to $0.01\text{m} \times 0.06\text{m} \times 0.06\text{m}$, the nonlinear resonator is at the centroid of the element. It is found that increasing the rolling-ball mass could decrease the frequency of local resonance band-gap for low-frequency, the central frequency of the band-gap is reduced from 14Hz to 10Hz. The rolling-ball mass of the resonator has minimal effect on the Bragg band-gap at high frequencies. Increasing the mass of the rolling-ball could decrease the resonance frequency of the corresponding nonlinear resonator, and the resulting local resonance band-gap shift to the low frequency. The position of the local resonance band-gap can be controlled by the change of the rolling-ball mass of the resonator in the unit. Therefore, according to the vibration response of different structures, appropriate mass rolling-balls can be selected to control the position of the band-gap, aiming at suppressing the vibration at a certain frequency by adjusting the band-gap. The nonlinear resonator can flexibly adjust the band-gap, which is a promising method for vibration suppression design.

4.3. Effects of cavity mass

The mass of the spherical magnetic cavity also has an important effect on the band-gap of wave propagation, and the mass of the spherical magnetic cavity is related to the size of the spherical magnetic cavity. **Fig. 14** shows the effects of mass of the spherical magnetic cavity. Increasing size of the spherical magnetic cavity has little effect on the local resonance band-gap caused by resonator resonance, but could significantly reduce the frequency of the Bragg band-gap and increase the bandwidth (the center frequency of the Bragg band-gap decreases from 53Hz to 47Hz, and the Bragg bandwidth increases from 2.5Hz to 10Hz), which restrain the propagation of elastic wave in more frequency range. By adjusting the size of the metamaterial beam spherical cavity, the band-gap width of the high frequency band can be expanded, while the vibration of the frequency range corresponding to the band-gap can be suppressed. In conclusion, the larger size of the spherical cavity in the metamaterial beam, the more reduction of vibration propagation are achieved.

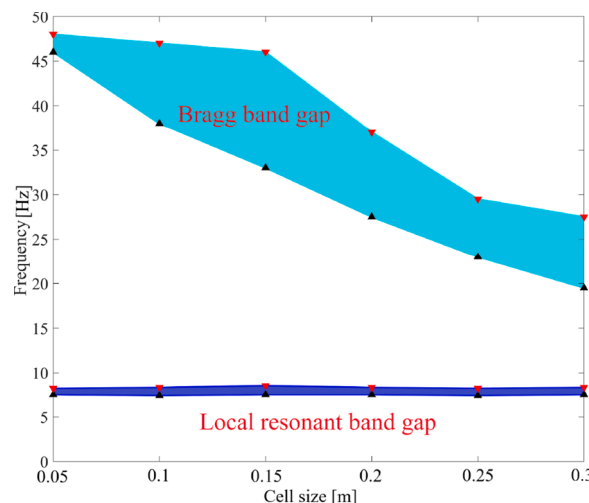


Fig. 12. Effect of unit cell size on band-gap.

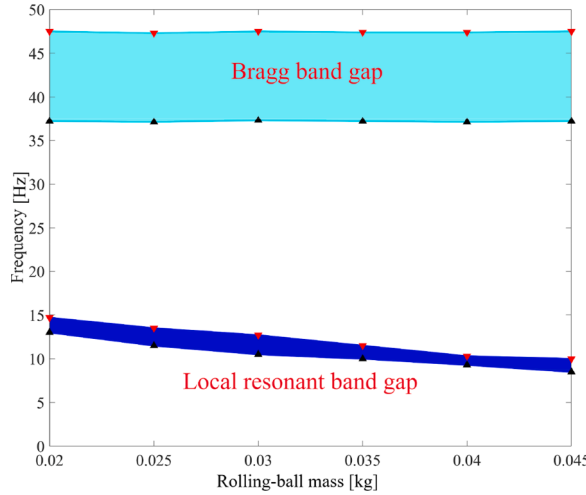


Fig. 13. Effects of rolling-ball mass in each nonlinear resonator.

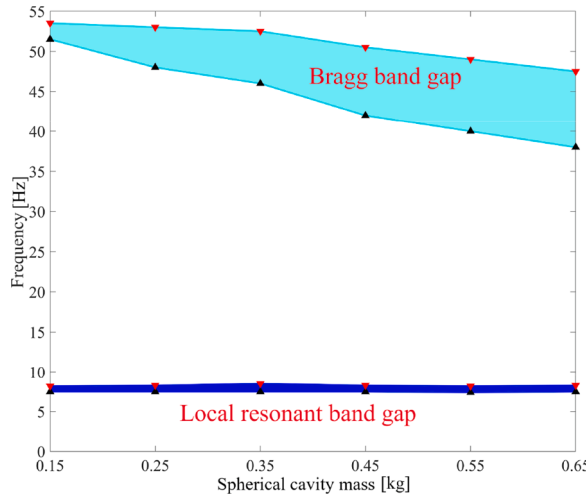


Fig. 14. Effects of mass of spherical magnetic cavity.

5. Experimental investigations

To observe the Bragg band-gap and low frequency local resonant band-gap of the metamaterial beam with nonlinear resonators, the rubber is used to construct the metamaterial beam, and the rolling-ball bearing is positioned into a spherical cavity to form a nonlinear resonator in paper. Frequency responses of displacement for the metamaterial beam are examined by harmonic excitation.

5.1. Static testing of the material parameters

To measure the frequency responses of displacement for the metamaterial beam, the material parameters of the experimental rubber body should be determined before the experiment. Compared with the traditional ABS or metal materials, the rubber has lower Young's modulus, and better vibration absorption. The rubber has better vibration reduction outside the band-gap frequency.

However, the rubber doping different materials has different properties. To determinate Young's modulus of the rubber, the stretching method is applied. The experimental photograph of the Young's modulus testing for the rubber is shown in Fig. 15. The ends of the test piece are fixed with clamp, and weights is suspended below for 15 minutes. The deformation of the rubber could be calculated by

$$E_r = \frac{P_0 g L_1}{b_0 h_0 \Delta L} \quad (26)$$

where $\Delta L = L_2 - L_1$, P_0 is the sum of the mass of the weights and the string, b_0 is the width of the rubber piece, h_0 is the thickness of the

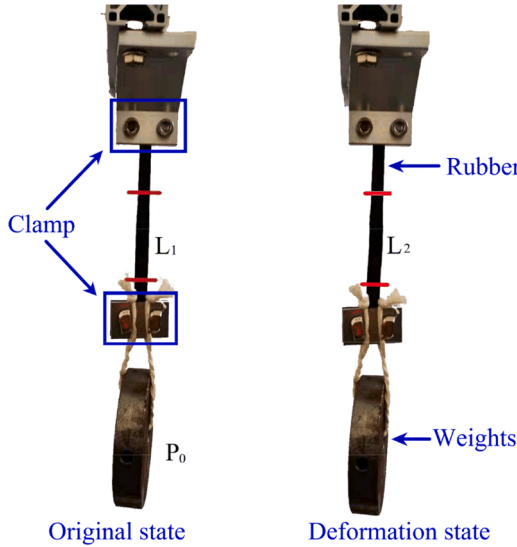


Fig. 15. The experimental photograph of the Young's modulus testing.

rubber piece.

The properties of a test piece are measured for three times. The results are shown in the [Table 2](#). During multiple measurements of each test piece, Young's modulus E_r is 761761Pa. The density of the rubber can be obtained, $\rho_r = 1810\text{kg/m}^3$.

5.2. Frequency responses of the metamaterial beam under transverse excitation

[Fig. 16](#) shows the experimental schematic and photograph of the transverse excited metamaterial beam with additional nonlinear resonators, the free boundary of the metamaterial beam is produced by hanging them on the support with cotton ropes. This experiment mainly concerns the dynamic behaviors of the metamaterial beam and validates the theoretical performance of the vibration isolation. The metamaterial beam is connected to the shaker that could produce a harmonic excitation.

To avoid the torque generated by the metamaterial beam, the excitation point at the middle of the metamaterial beam. The response of the other end are recorded at each frequency. [Table 3](#) shows the instruments used in the experiment. [Table 4](#) shows the parameters of the metamaterial beam. In the photograph, the red arrows point in the direction of the profile view of the unit cell.

The vibration isolation efficiency in the band-gap μ_{BGIE} is introduced in this experiment to quantitatively reflect the vibration isolation efficiency of each band-gap.

$$\mu_{\text{BGIE}} = \left(1 - \frac{A_{\text{Orms}}}{A_{\text{Arms}}} \right) \times 100\% \quad (27)$$

where A_{Orms} is the root mean square of n times responses near the optimal frequency for vibration suppression band-gap; A_{Arms} is the root mean square of n times excitations near the corresponding frequency.

In the experiment, the sweep frequency range of 5-100Hz is divided into two parts: the displacement excitation is used in the range of 5-20Hz, the acceleration excitation is applied in the range of 20-100Hz. The displacement responses at the end of the metamaterial beam are recorded by the accelerometers. [Fig. 17](#) shows frequency responses of displacement at these two sweeping frequency ranges.

[Fig. 17\(a\)](#) shows the displacement response at the end of the metamaterial beam, which is suppressed near the resonance frequency (6Hz-7Hz) of the additional resonator. In [Table 5](#), the vibration suppression efficiency near the resonance frequency of the resonator can reach 73.52%. Increasing the excitation frequency and amplitude, the vibration of the resonance sphere increases in the cavity, but the vibration could not be suppressed effectively. The local resonance band-gap can only produce near the resonance frequency of the resonator. [Fig. 17\(b\)](#) shows the displacement at the response is significantly smaller than that at the excitation in the frequency range of 45Hz-65Hz and the response is stable in this frequency range. The reason for this is that the Bragg band-gap could be generated by periodic cavities in the rubber body of a metamaterial beam, the existence of the band-gap enables the vibration to be stably suppressed in this frequency range. In [Table 5](#), the vibration suppression efficiency within the Bragg band-gap reaches 81.34%.

The expression for the bending wave number of the metamaterial beam can be given by

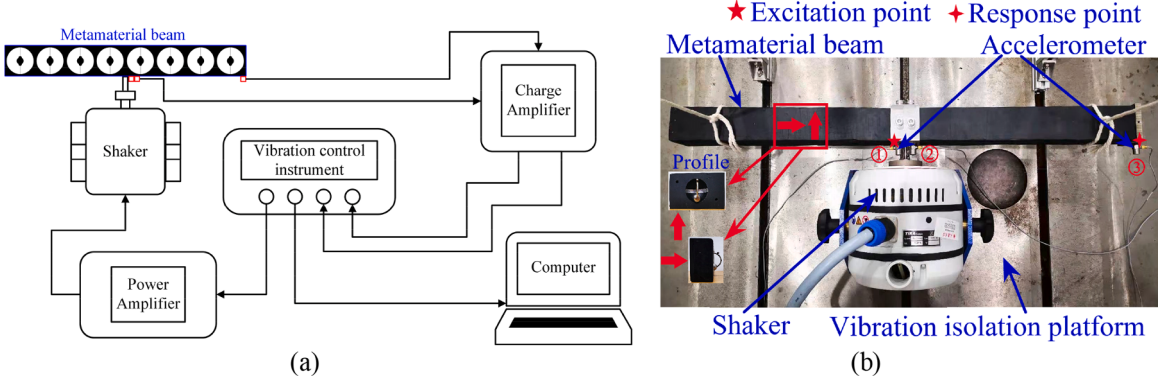
$$k_b = \left[\frac{\rho_{lr} A_r (2\pi f)^2}{E_r I_r} \right]^{1/4} \quad (28)$$

The Bragg condition for a one-dimensional periodic structure can be written as

Table 2

Testing data of the rubber properties.

$P_0 = 1.009\text{kg}$	L_1	L_2	ΔL	
$g = 9.8\text{m/s}^2$	No.1	0.05179m	0.06497m	$E_{11} = 7.7 \times 10^5\text{Pa}$
$b_0 = 0.01\text{m}$	No.2	0.05173m	0.06512m	$E_{12} = 7.6 \times 10^5\text{Pa}$
$h_0 = 0.005\text{m}$	No.3	0.05125m	0.06487m	$E_{13} = 7.4 \times 10^5\text{Pa}$

**Fig. 16.** The experimental schematic (a) and photograph of the transverse excited metamaterial beam (b).**Table 3**

Experiment instruments.

Instruments name	Version	Quantity	Manufacturer	Country
Shaker	TV-51140	1	TIRA	Germany
Accelerometer	352C03	3	PCB	USA
Vibration controller	VT-9008	1	ECON	China

Table 4

Parameters of the experimental metamaterial beam.

Item	Notation	Value
length	$l_r [\text{m}]$	0.1
cross-sectional area	$A_r [\text{m}^2]$	0.0036
density of material	$\rho_r [\text{kg/m}^3]$	1810
Young's modulus	$E_r [\text{Pa}]$	761761
spherical cavity radius	$R_{nr} [\text{m}]$	0.02
rolling-ball radius	$r_r [\text{m}]$	0.007
density of spherical material	$\rho_{1r} [\text{kg/m}^3]$	7780
inertia moment	$I_r [\text{m}^4]$	1.08×10^{-6}

$$l_r = \frac{n\pi}{k_b}, \quad n = 1, 2, 3, \dots \quad (29)$$

The frequency of the Bragg band-gap is

$$f_{B,n} = \frac{1}{2\pi} \left(\frac{n\pi}{l_r} \right)^2 \sqrt{\frac{E_r I_r}{\rho_{1r} A_r}}, \quad n = 1, 2, 3, \dots \quad (30)$$

Eq. (30) represents the relationship between the Bragg band-gaps and the metamaterial parameters. The frequencies of the Bragg band-gaps depend on both the parameters of the metamaterial beam and unit cell constant l_r . But the frequencies are not related to the periodical arrayed resonator. In conclusion, the Bragg band-gaps of lower frequency range in metamaterial beams generally required a larger unit cell constant for a given beam structure.

In this case, the first Bragg frequency of the metamaterial beam can be given by

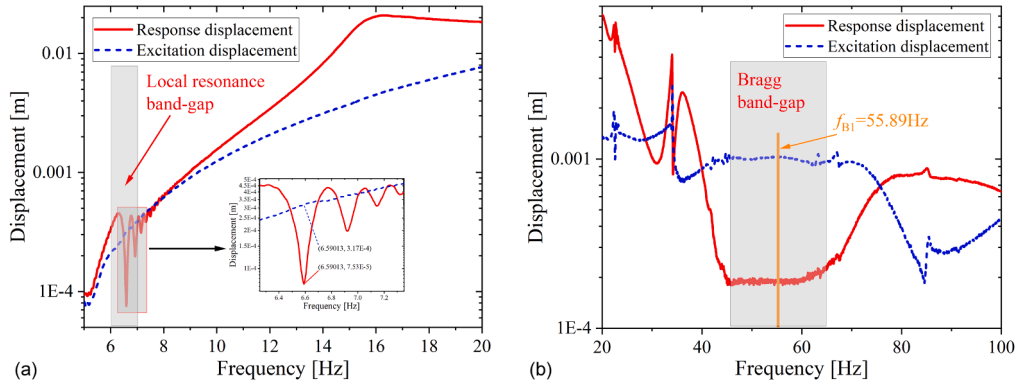


Fig. 17. Frequency response of the displacement under transverse excitation: (a) harmonic displacement excitation; (b) acceleration excitation.

Table 5

Vibration isolation efficiency in band-gap.

Band-gaps	A _{Arms} [m]	A _{Orms} [m]	μ _{BGE}
Local resonant band-gap	0.000318	0.000083	73.82%
Bragg band-gap	0.001026	0.000191	81.34%

$$f_{B1} = \frac{1}{2\pi} \left(\frac{\pi}{l_r} \right)^2 \sqrt{\frac{E_r I_r}{\rho_{lr} A_r}} = 55.9 \text{Hz} \quad (31)$$

Fig. 17(b) shows the Bragg band-gap locates near the Bragg frequency. The vibration-suppression of Bragg band-gaps validated by the experiment are larger than the frequency ranges calculated for the metamaterial beam. The errors could be produced during the processing of the rubber spherical cavity. Both experimental and theoretical results show that the designed metamaterial beam can produce two types of band-gaps, which could suppress the propagation of vibration. The measured band-gap characteristics agree with the theoretical results.

6. Conclusion

This paper presents a dual-functional metamaterial design with cavity mass and energy harvester, for both suppressing wave propagation of low-frequency and harvesting energy. This novel design arranges a periodic array of nonlinear electrical energy harvesters, realized by implanting a rolling-ball with coils into a spherical magnetic cavity, on a beam to create band-gaps for wave isolation and produce electrical energy. The amplitude frequency response and amplitude-excitation amplitude-response of a nonlinear resonator highlight the nonlinear characteristics of this dual-functional metamaterial. The dynamical equation is established for dual-functional metamaterial under transverse excitation. The Extended Bloch's theorem is applied to give the dispersion relation. The wave propagation of a beam composed of this dual-functional metamaterial are analyzed via finite element method. Numerical results obtained by finite element method supported the analytical results. Moreover, the transverse excited dual-functional metamaterial experimental rig designed to validate the vibration isolation band-gap characteristics of the metamaterial beam.

The conclusions can be summarized as follows: The response peak generated during wave propagation can be effectively suppressed in the frequency range of forbidden band. Moreover, the generated band-gaps shift to lower frequencies, which could lead to reduce the transmitted vibration during wave propagation. Simultaneously, the energy generated when the rolling-ball slides in the nonlinear resonator can be harvested. The harvested power is considerable at the local resonant band-gap. Parameter study demonstrates that increasing the cell size and increasing cavity mass of the resonator has minimal effect on the frequency range of the local resonance band-gap, but it will reduce the frequency of the Bragg band-gap and increase the bandwidth, which can better inhibit the propagation of elastic waves at low frequencies; Increasing the mass of the rolling-ball in the resonator can significantly reduce the frequency of the local resonance band-gap caused by resonance. Finally, the experimental results are in agreement with the theoretical results.

In summary, dual-functional acoustic metamaterials with nonlinear energy harvesters have better vibration suppression than that of linear metamaterials, and simultaneously are capable of vibration energy harvesting. Therefore, the presented work has laid the foundation of dual-functional metamaterials for the broadband vibration isolation of low-frequency.

Funding

This study was funded by the National Natural Science Foundation of China (Grant Nos. 11872037, 11872159, and 11572182) and the Innovation Program of Shanghai Municipal Education Commission (Grant No. 2017-01-07-00-09-E00019).

Data Availability

The data used to support the findings of this study are available from the corresponding author upon request.

Credit author statement

Ze-Qi Lu: Research concept, design, Writing the article; **Long Zhao:** Data analysis and interpretation, **Hu Ding:** Collection; **Li-Qun Chen:** Critical revision of the article, Final approval of article.

Declaration of Competing Interest

We wish to confirm that there are no known conflicts of interest associated with this publication. We confirm that the manuscript has been read and approved by all named authors and that there are no other persons who satisfied the criteria for authorship but are not listed. We further confirm that the order of authors listed in the manuscript has been approved by all of us.

References

- [1] Y.B. Li, Y. Shen, S.Y. Cao, X.S. Zhang, Y.D. Meng, Thermally triggered tunable vibration mitigation in Hoberman spherical lattice metamaterials, *Appl. Phys. Lett.* 114 (2018), 191904, <https://doi.org/10.1063/1.5092423>.
- [2] Q. Geng, T.Y. Cai, Y.M. Li, Flexural wave manipulation and energy harvesting characteristics of a defect phononic crystal beam with thermal effects, *J. Appl. Phys.* 125 (2019), 035103, <https://doi.org/10.1063/1.5063949>.
- [3] Y.Y. Chen, M.V. Barnhart, J.K. Chen, G.K. Hu, C.T. Sun, G.L. Huang, Dissipative elastic metamaterials for broadband wave mitigation at subwavelength scale, *Composite Structures.* 136 (2016) 358–371. <https://doi.org/10.1016/j.compstruct.2015.09.048>.
- [4] E. Kim, J.Y. Yang, Wave propagation in single column woodpile phononic crystals: formation of tunable band gaps, *J. Mech. Phys. Solids* 71 (2014) 33–45, <https://doi.org/10.1016/j.jmps.2014.06.012>.
- [5] S.B. Li, Y.H. Dou, T.N. Chen, J.N. Xu, B. Li, F. Zhang, Designing a broad locally-resonant bandgap in a phononic crystals, *Phys. Lett. A* 383 (2019) 1371–1377, <https://doi.org/10.1016/j.physleta.2019.01.061>.
- [6] C Nimmagadda, K.H. Matlack, Thermally tunable band gaps in architected metamaterial structures, *J. Sound Vib.* 439 (2019) 29–42, <https://doi.org/10.1016/j.jsv.2018.09.053>.
- [7] Y.K. Dong, H. Yao, J. Du, J.B. Zhao, C. Ding, Research on bandgap property of a novel small size multi-band phononic crystal, *Phys. Lett. A* 383 (2019) 283–288, <https://doi.org/10.1016/j.physleta.2018.10.042>.
- [8] J. Shim, P. Wang, K. Bertoldi, Harnessing instability-induced pattern transformation to design tunable phononic crystals, *Int. J. Solids Struct.* 58 (2015) 52–61, <https://doi.org/10.1016/j.ijsolstr.2014.12.018>.
- [9] R. Zhu, X.N. Liu, G.K. Hu, C.T. Sun, G.L. Huang, Negative refraction of elastic waves at the deep-subwavelength scale in a single-phase metamaterial, *Nat. Commun.* 5 (2014) 5510, <https://doi.org/10.1038/ncomms6510>.
- [10] K.C. Chuang, Z.Q. Zhang, H.X. Wang, Experimental study on slow flexural waves around the defect modes in a phononic crystal beam using fiber Bragg gratings, *Phys. Lett. A* 380 (2016) 3963–3969, <https://doi.org/10.1016/j.physleta.2016.09.055>.
- [11] G.C. Ma, P. Sheng, Acoustic metamaterials: From local resonances to broad horizons, *Sci. Adv.* 2 (2016), e1501595, <https://doi.org/10.1126/sciadv.1501595>.
- [12] S.A. Cummer, J. Christensen, A. Alù, Controlling sound with acoustic metamaterials, *Nat. Rev. Mater.* 1 (2016) 16001, <https://doi.org/10.1038/natrevmat.2016.1>.
- [13] M.R. Haberman, M. Guild, Acoustic metamaterials, *Phys. Today* 69 (6) (2016) 42, <https://doi.org/10.1063/PT.3.3198>.
- [14] M. Carrara, M.R. Cacan, J. Toussaint, M.J. Leamy, M. Ruzzene, A. Erturk, Metamaterial-inspired structures and concepts for elastoacoustic wave energy harvesting, *Smart Mater. Struct.* 22 (2013), 065004, <https://doi.org/10.1088/0964-1726/22/6/065004>.
- [15] M. Miniaci, A. Krushynska, F. Bosia, N.M. Pugno, Large scale mechanical metamaterials as seismic shields, *New J. Phys.* 18 (2016), 083041, <https://doi.org/10.1088/1367-2630/18/8/083041>.
- [16] Y.Y. Chen, M.V. Barnhart, J.K. Chen, G.K. Hu, C.T. Sun, G.L. Huang, Dissipative elastic metamaterials for broadband wave mitigation at subwavelength scale, *Compos. Struct.* 136 (2016) 358–371, <https://doi.org/10.1016/j.compstruct.2015.09.048>.
- [17] S.C. Kwon, M.S. Jo, H.U. Oh, Numerical investigation of complex system for electrical energy harvesting and vibration isolation, *Int. J. Aeronaut. Space Sci.* 42 (2014) 648–653.
- [18] S.C. Kwon, H.U. Oh, Experimental validation of satellite micro-jitter management strategy in energy harvesting and vibration isolation, *Sensors Actuators A-Phys.* 249 (2016) 172–185.
- [19] Y.T. Choi, N.M. Wereley, Self-powered magnetorheological dampers, *J. Acoust. Vibr.* 131 (2009), 044501, <https://doi.org/10.1115/1.3142882>.
- [20] R.B. Davis, M.D. McDowell, Combined Euler column vibration isolation and energy harvesting, *Smart Mater. Struct.* 26 (2017), 055001, <https://doi.org/10.1088/1361-665X/aa6721>.
- [21] Z.Q. Lu, D. Shao, Z.W. Fang, H. Ding, L.Q. Chen, Integrated vibration isolation and energy harvesting via a bistable piezo-composite plate, *J. Vib. Control* 26 (2020) 779–789, <https://doi.org/10.1177/1077546319889815>.
- [22] J. Hobeck, D. Inman, Simultaneous passive broadband vibration suppression and energy harvesting with multifunctional metastructures. SPIE Smart Structures and Materials + Nondestructive Evaluation and Health Monitoring, in: Society of Photo-Optical Instrumentation Engineers (SPIE) Conference Series. 101720K, 2017, <https://doi.org/10.1117/12.2260093>.
- [23] M. Bukhari, O. Barry, Simultaneous energy harvesting and vibration control in a nonlinear metastructure: A spectro-spatial analysis, *J. Sound Vib.* 473 (2020), 115215, <https://doi.org/10.1016/j.jsv.2020.115215>.
- [24] Y.W. Zhang, C. Su, Z.Y. Ni, J. Zang, L.Q. Chen, 2019. A multifunctional lattice sandwich structure with energy harvesting and nonlinear vibration control, *Composite Structures.* 221, 110875. <https://doi.org/10.1016/j.compstruct.2019.04.047>.
- [25] Z.Y. Liu, X.X. Zhang, Y.W. Mao, Y.Y. Zhu, Z.Y. Yang, C.T. Chan, P. Sheng, Locally resonant sonic materials, *Science* 289 (2000) 1734, <https://doi.org/10.1126/science.289.5485.1734>.
- [26] Y.Y. Chen, G.L. Huang, X.M. Zhou, G.K. Hu, C.T. Sun, Analytical coupled vibroacoustic modeling of membrane-type acoustic metamaterials: membrane model, *J. Acoust. Soc. Am.* 136 (2014) 969–979, <https://doi.org/10.1121/1.4901706>.
- [27] S.H. Lee, C.M. Park, Y.M. Seo, Z.G. Wan, C.K. Kim, Acoustic metamaterial with negative modulus, *J. Phys. A* 21 (2009), 175704, <https://doi.org/10.1088/0953-8984/21/17/175704>.
- [28] J.J. Guo, J.Z. Cao, Y. Xiao, H.J. Shen, J.H. Wen, Interplay of local resonances and Bragg band gaps in acoustic waveguides with periodic detuned resonators, *Phys. Lett. A* 384 (2020), 126253, <https://doi.org/10.1016/j.physleta.2020.126253>.
- [29] S.R. Wen, Y.H. Xiong, S.M. Hao, F.M. Li, C.Z. Zhang, Enhanced band-gap properties of an acoustic metamaterial beam with periodically variable cross-sections, *Int. J. Mech. Sci.* 166 (2020), 105229, <https://doi.org/10.1016/j.ijmecsci.2019.105229>.

- [30] A. Pelat, T. Gallot, F. Gautier, On the control of the first Bragg band gap in periodic continuously corrugated beam for flexural vibration, *J. Sound Vib.* 446 (2019) 249–262, <https://doi.org/10.1016/j.jsv.2019.01.029>.
- [31] Y.Z. Wang, F.M. Li, Wang Y.S, Influences of active control on elastic wave propagation in a weakly nonlinear phononic crystal with a monoatomic lattice chain, *Int. J. Mech. Sci.* 106 (2016) 357–362, <https://doi.org/10.1016/j.ijmecsci.2015.12.004>.
- [32] H.W. Sun, X.W. Du, P.F. Pai, Theory of Metamaterial Beams for Broadband Vibration Absorption, *J. Intell. Mater. Syst. Struct.* 21 (2010) 1085, <https://doi.org/10.1177/1045389X10375637>.
- [33] Y.Z. Liu, D.L. Yu, L. Li, H.G. Zhao, J.H. Wen, X.S. Wen, Design guidelines for flexural wave attenuation of slender beams with local resonators, *Phys. Lett. A* 362 (2007) 344–347, <https://doi.org/10.1016/j.physleta.2006.10.056>.
- [34] S. El-Borgi, R. Fernandes, P. Rajendran, R. Yazbeck, J.G. Boyd, D.C. Lagoudas, Multiple bandgap formation in a locally resonant linear metamaterial beam: Theory and experiments, *J. Sound Vib.* 488 (2020), 115647, <https://doi.org/10.1016/j.jsv.2020.115647>.
- [35] Y.L. Huang, J. Li, W.Q. Chen, R.H. Bao, Tunable bandgaps in soft phononic plates with spring-mass-like resonators, *Int. J. Mech. Sci.* 151 (2019) 300–313, <https://doi.org/10.1016/j.ijmecsci.2018.11.029>.
- [36] P.F. Pai, H. Peng, S.Y. Jiang, Acoustic metamaterial beams based on multi-frequency vibration absorbers, *Int. J. Mech. Sci.* 79 (2014) 195–205, <https://doi.org/10.1111/12.2045061>.
- [37] K. Wang, J.X. Zhou, Q. Wang, H.J. Ouyang, D.L. Xu, Low-frequency band gaps in a metamaterial rod by negative-stiffness mechanisms: Design and experimental validation, *Appl. Phys. Lett.* 114 (2019), 251902, <https://doi.org/10.1063/1.5099425>.
- [38] Z.J. Wu, W.Y. Liu, F.M. Li, C.Z. Zhang, 2019. Band-gap property of a novel elastic metamaterial beam with X-shaped local resonators, *Mechanical Systems and Signal Processing*, 134, 106357. <https://doi.org/10.1016/j.ymssp.2019.106357>.
- [39] J.X. Zhou, L.L. Dou, K. Wang, D.L. Xu, H.J. Ouyang, A nonlinear resonator with inertial amplification for very low-frequency flexural wave attenuations in beams, *Nonlinear Dyn.* 96 (2019) 647–665, <https://doi.org/10.1007/s11071-019-04812-1>.
- [40] J.X. Zhou, K. Wang, D.L. Xu, H.J. Ouyang, Local resonator with high-static-low-dynamic stiffness for lowering band gaps of flexural wave in beams, *J. Appl. Phys.* 121 (2017), 044902, <https://doi.org/10.1063/1.4974299>.
- [41] K. Wang, J.X. Zhou, D.L. Xu, H.J. Ouyang, Lower band gaps of transverse wave in a one-dimensional periodic rod by exploiting geometrical nonlinearity, *Mechanical Systems and Signal Processing*, 124 (2019) 664–678. <https://doi.org/10.1016/j.ymssp.2019.02.008>.
- [42] T. Wang, M.P. Sheng, Q.H. Qin, Multi-flexural band gaps in an Euler-Bernoulli beam with lateral local resonators, *Phys. Lett. A* 380 (2016) 525–529, <https://doi.org/10.1016/j.physleta.2015.12.010>.
- [43] Z. Zhang, T.J. Li, Z.W. Wang, Y.Q. Tang, Band gap characteristics of flexural wave of two-dimensional periodic frame structure composed of locally resonant composite beam, *Mechanical Systems and Signal Processing*, 131 (2019) 364–380. <https://doi.org/10.1016/j.ymssp.2019.05.060>.
- [44] Y.Y. Chen, G.K. Hu, G.L. Huang, A hybrid elastic metamaterial with negative mass density and tunable bending stiffness, *J. Mech. Phys. Solids* 105 (2017) 179–198, <https://doi.org/10.1016/j.jmps.2017.05.009>.
- [45] O.V. Gendelman, Transition of energy to a nonlinear localized mode in a highly asymmetric system of two oscillators, *Nonlinear Dyn.* 25 (2001) 237–253, <https://doi.org/10.1023/A:1012967003477>.
- [46] N.E. Wierschem, Targeted energy transfer using nonlinear energy sinks for the attenuation of transient loads on building structures, *University of Illinois at Urbana Champaign, Illinois*, 2014.
- [47] L.I. Manevitch, G. Sigalov, F. Romeo, L.A. Bergman, A. Vakakis, Dynamics of a linear oscillator coupled to a bistable light attachment: Numerical study, *J. Comput. Nonlinear Dyn.* 10 (2015), 011007, <https://doi.org/10.1115/1.4027224>.
- [48] L.I. Manevitch, G. Sigalov, F. Romeo, L.A. Bergman, A. Vakakis, Dynamics of a linear oscillator coupled to a bistable light attachment: Analytical study, *J. Appl. Mech.* 81 (2014), 041011, <https://doi.org/10.1115/1.4025150>.
- [49] C.M. Donahue, P. Anzel, L. Bonanomi, T.A. Keller, C. Daraio, Experimental realization of a nonlinear acoustic lens with a tunable focus, *Appl. Phys. Lett.* 104 (2014), 014103, <https://doi.org/10.1063/1.4857635>.
- [50] J.Y. Li, Y. Gao, J.P. Huang, A bifunctional cloak using transformation media, *J. Appl. Phys.* 108 (2010), 074504, <https://doi.org/10.1063/1.3490226>.
- [51] X.Y. Shen, Y. Li, C.R. Jiang, Y.S. Ni, J.P. Huang, Thermal cloak-concentrator, *Appl. Phys. Lett.* 109 (2016), 031907, <https://doi.org/10.1063/1.4959251>.
- [52] M. Wiercigroch, A. Najdecka, V. Vaziri, Nonlinear dynamics of pendulums system for energy harvesting, *Vibr. Probl. ICOVP* (2011) 35–42, https://doi.org/10.1007/978-94-007-2069-5_4.
- [53] M. Wiercigroch, A new concept of energy extraction from oscillations via pendulum systems, *UK Patent Appl.* (2009).
- [54] A. Najdecka, S. Narayanan, M. Wiercigroch, Rotary motion of the parametric and planar pendulum under stochastic wave excitation, *Int. J. Non Linear Mech.* 71 (2015) 30–38, <https://doi.org/10.1016/j.ijnonlinmec.2014.12.008>.
- [55] M. Malodovan, Sound and heat revolutions in phononics, *Nature* 503 (2013) 209–217, <https://doi.org/10.1038/nature12608>.